Chapter 4

Introduction to Optical/Near-Infrared Interferometry

Fabien Malbet

Fabien.Malbet@obs.ujf-grenoble.fr

LAOG, BP 53, F-38041 Grenoble Cedex 09, France

4.1 Introduction

This chapter is focused on optical (i.e. visible and infrared) interferometry with in mind the comparison of this technique with radio interferometry developed in the other chapters of this book. The objective is to give some keys to understand how optical interferometers works. I present first a small history of optical interferometry followed by a census of interferometers in operation or in construction (Sect. 4.1). Section 4.2 discusses the common points and main differences between optical and radio interferometry at millimeter wavelengths. Then I describe how an optical interferometer works (Sect. 4.3) at the system level and at the signal detection level (Sect. 4.4). Finally I present in Sect. 4.5 the main limitations that optical interferometry faces like the atmospheric turbulence and other sources of noise in the measured signal.

4.1.1 Brief history of optical interferometry

Stellar interferometry has been first proposed by Fizeau in 1868. At that time, the phenomenon of light interference is already well studied and the physicists know that the contrast of the fringes depends on the geometry of the source. [Fizeau 1868] suggests to deduce the star diameter from the extinction of the fringe contrast with widely separated slits. [Stéphan.1873] installs a mask with two apertures on the 0.80-m telescope of the Marseille observatory to test Fizeau's method. He detects fringes but the contrast of fringes do not decrease with the aperture distance. He concludes that stars must be smaller than 0.158 arcsec.

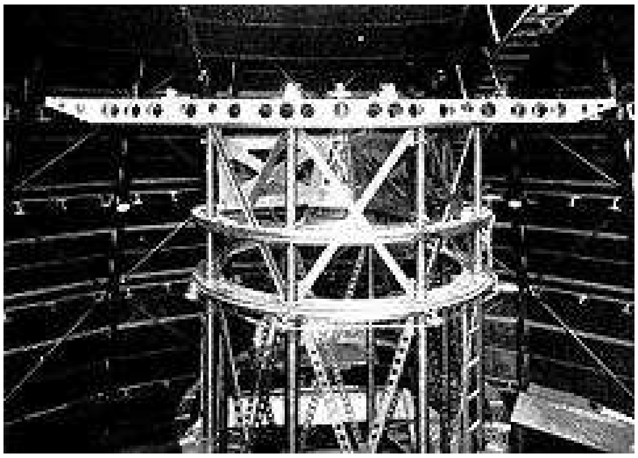

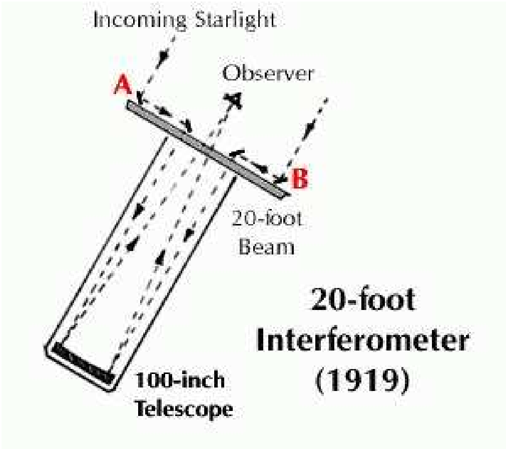

Figure 4.1: Michelson 20-foot interferometer installed on 100-in telescope at Mount Wilson.

Following his own work on the measurement of light speed, Michelson seems to have independently discovered optical interferometry in the 1890's. In order to span a large range of baselines, he and Pease install a 20-foot metal beam above the 100-in telescope of Mount Wilson. Two mirrors inclined by 45 degrees send the light to the middle of the telescope where two other mirrors inject the light in the telescope. The interferometric fringes are formed at the focus of the telescope (see Fig. 4.1). By translating the outside mirrors, the baseline changes and therefore also the contrast of the fringes. In the 1920's, [Michelson & Pease 1921] measure the first diameters of stars that required baselines longer than 3m. To extend these first results, Pease builds a stand-alone interferometer on a 50-foot metal beam, but fails in getting calibrated results because of the unexpected importance of mechanical flexures.

During almost 50 years, direct detection interferometry stalled. [Hanbury Brown & Twiss 1956] invented intensity interferometry which is limited to a small handset of bright sources. Interferometry had a new birth in the mid-1970's with the advent of new technology: detectors, actuators, servo-control, etc. [Labeyrie 1975] was the first to directly combine the light from two separated telescopes in the optical range. Since that time several interferometers with relatively small apertures have been built and operated. A list of current and future interferometers is given in Table 4.1 and commented in next section.

In 1988, the heterodyne techniques used in the radio domain was first implemented in an operating interferometer at 10 μm by the *Infrared Spatial Interferometer* (ISI, [Danchi et al. 1988]).

4.1.2 Current and future optical interferometers

Current interferometers (see list in Table 4.1) are composed of relatively small telescopes, with diameters ranging between 15 centimeters to 1.5 meters. The number of telescopes used to combine the light is usually two, but if two facilities work routinely with 3 or more apertures (COAST and NPOI). The maximum baseline length ranges between a few meters up to several hundreds of meters (e.g. SUSI). Almost each interferometer has its own beam combination scheme (see Sect. 4.4.1). They work either in the visible ($0.4 - 1$ μm) or the infrared ($1 - 10$ μm) domains.

Each interferometer has been designed with one main astrophysical objective: synthetic aperture imaging (COAST, UK), high resolution spectroscopy in the visible (GI2T, France), high accuracy measurement in the near-infrared (IOTA, USA), high resolution spectroscopy in the thermal infrared (ISI, USA), wide angle astrometry (NPOI, USA), narrow angle astrometry and phase reference (PTI, USA), stellar astrophysics in the visible (SUSI, Australia). CHARA (USA), which obtained its first fringes at the end of 1999, aims at binary observations and synthetic aperture imaging.

The new generation consists of interferometers with very large telescopes: the VLTI with 4×8-m

Table 4.1: List of ground-based optical interferometers in operation or in construction.

Name	**Facility**	**# tel.**	$\mathcal{D}$(m)	$\mathcal{B}$ (m)
COAST	Cambridge Optical Aperture Synthesis Telescope	5	0.4	20
GI2T	Grand Interféromètre à 2 Télescopes	2	1.52	65
IOTA	Infrared & Optical Telescope Array	2*	0.4	38
ISI	Infrared Spatial Interferometer	2*	1.65	85*
NPOI	Naval Prototype Optical Interferometer	3*	0.12*	35*
PTI	Palomar Testbed Interferometer	3	0.4	110
SUSI	Sidney University Stellar Interferometer	2	0.14	640
CHARA	Center for High Angular Resolution Astrophysics	6	1	350
KI-main	Keck Interferometer main array	2	10	60
KI-outriggers	Keck Interferometer auxiliary array	4	1.8	140
VLTI/VIMA	Very Large Telescope Interferometer main array	4	8	130
VLTI/VISA	Very Large Telescope Interferometer sub-array	3	1.8	200
LBT	Large Binocular Telescope	2	8.4	23

* upgrade in progress

telescopes, the *Keck Interferometer* with 2×10-m telescopes and the LBT with two 8-m telescopes. Their main objective is the gain in flux sensitivity which will allow for the first time the study of extra-galactic sources. Both the VLTI and the *Keck Interferometer* are supplemented by auxiliary 1.8-m telescopes, that are still larger than the largest apertures in the previous generation of interferometers.

4.2 Optical versus millimeter radio interferometry

Optical and millimeter radio interferometry are essentially the same technique used in two different wavelength domains. Although they share the same fundamentals and the same objectives (see Sect. 4.2.1), their implementations can exhibit some significative differences (see Sect. 4.2.2). More details are given in Chap. 21.

4.2.1 Common issues

Both optical and millimeter interferometers study the coherence of the electric field by the mean of separated apertures, called telescopes, siderostats or antennas. The principle of these two techniques is based on the Zernike-Van Cittert theorem, i.e. the degree of coherence of the light is directly related to the Fourier transform of the spatial distribution of the intensity of the observed object [Goodman 1985].

By using separated apertures, both techniques achieve high angular resolution observation, with a resolution tens to hundreds of time larger than single aperture in the same wavelength domain. They therefore face similar difficulties, since they both used diluted arrays and have to find the best array configurations to reach their respective objectives. Similarly to millimeter radio interferometry, optical interferometry has also to calibrate the measured complex visibilities.

When optical interferometry will become as mature as millimeter interferometry, one will probably use very similar algorithm to reconstruct images from the calibrated visibilities.

4.2.2 Main differences

The differences come mainly from the wavelength domains: the typical optical wavelength is 1 μm, which corresponds to a frequency of 300 THz to be compared with the typical millimeter radio wavelength of 1 mm and the corresponding 300 GHz frequency.

The first consequence is the actual angular resolution that can be achieved, defined by the fringe spacing $\lambda/\mathcal{B}$. The typical resolution reached in the optical domain is about 1 milli-arcsecond whereas in the millimeter domain, the Plateau de Bure Interferometer (PdBI) reaches about 1 arcsecond. ALMA with its extended baselines will be able to get 0.03 arcsecond but the information will still be 100 times less resolved than with optical interferometers.

A second difference comes from the type of detection and beam combination. In millimeter interferometry, the signal detection occurs at the antenna level thanks to the heterodyne technique. The signal is coupled with a reference signal of high coherence and therefore one records the amplitude and the phase of the coming electric field. The signals from each antenna are then digitized and the combination takes place in the correlator (see first chapters of this book). An electronic phase delay is applied to take into account the difference in path length between two arms. In the optical domain, the heterodyne technique has been successful at 10 μm [Gay & Journet 1973, Johnson et al. 1974]. This technique however happens to be not sensitive. That is why optical interferometry is usually achieved by direct detection of interferences. The light beams are propagated to a central lab, where the optical path is equalized and are combined to form interferences before being detected. Since the detection techniques measure only the power of the electric field, one has to code the fringes either temporally or spatially (see Sect. 4.4.2). Finally the two techniques give different types of interferences: respectively multiplicative and additive. The heterodyne technique directly gives access to the electric field ψ_k for each aperture and therefore the interference signal is multiplicative (see also Chapter 2 and 21).

The quadratic detection in the direct technique gives additive interferences:

$$I_{kl} = <(\psi_k + \psi_l)(\psi_k + \psi_l)^* >= I_k + I_l + 2\sqrt{I_k I_l}\, v_{kl}\ \cos\phi_{kl}\,, \tag{4.1}$$

where $< ... >$ stands for a temporal average over a time long compared to the inverse frequency of the signal, I_k is the intensity of the k-th beam, and v_{kl} and ϕ_{kl} are respectively the amplitude and phase of the normalized visibility. One of the consequences is a different type of calibration process, another is that visibility unit is Jansky in the millimeter domain, whereas in the optical domain it is dimension-less, i.e. flux normalized.

A third and important difference is the influence of the atmosphere. In the optical domain the dominant effect is the corrugation of the wavefront. The spatial Fried's parameter, r_0, which corresponds to the spatial scale of the turbulence is smaller than the telescope size. Typical numbers are $0.1 - 0.2$ m in the visible and $0.5 - 1$ m in the near infrared. That is a reason why many interferometers have aperture diameters below 1 m (see Table 4.1). In the millimeter, r_0 is larger than the antenna sizes. The temporal Fried's parameter, t_0, which corresponds to the temporal scale of the turbulence is of the order of 10-100 ms in the optical versus several minutes in the millimeter. That is why it is possible to use phase referencing (phase calibration on a source with known phase) with radio interferometers by off-pointing the interferometer, when it is almost impossible to calibrate the phase in the optical. The only way to retrieve the phase is to measure closure phases with more than 3 apertures or to use a dual-beam interferometer and an accurate metrology like for narrow-angle astrometry (see Sect. 4.3.2). The fact that the phase is almost impossible to get in the optical makes therefore a large difference in the way the data are processed to obtain images.

A last difference is the type of noise encountered. The main source of noise in millimeter interferometry is the thermal noise. In optical interferometry, the three type of noises are the photon noise, the read-out noise of the detectors and the background noise, coming either from thermal emission or from the sky brightness. In addition, noise from the atmosphere turbulence, either photometric fluctuations or speckles, must be taken into account.

4.3 Description of optical interferometers

This section is dedicated to the overview of interferometric systems. We first go through the functional description of a typical optical interferometer, then describe the different types of interferometers with specific objectives.

4.3.1 Functional description

Optical interferometry aims at measuring the complex degree of coherence of the observed object. To achieve such a goal, optical interferometers require the following functionalities:

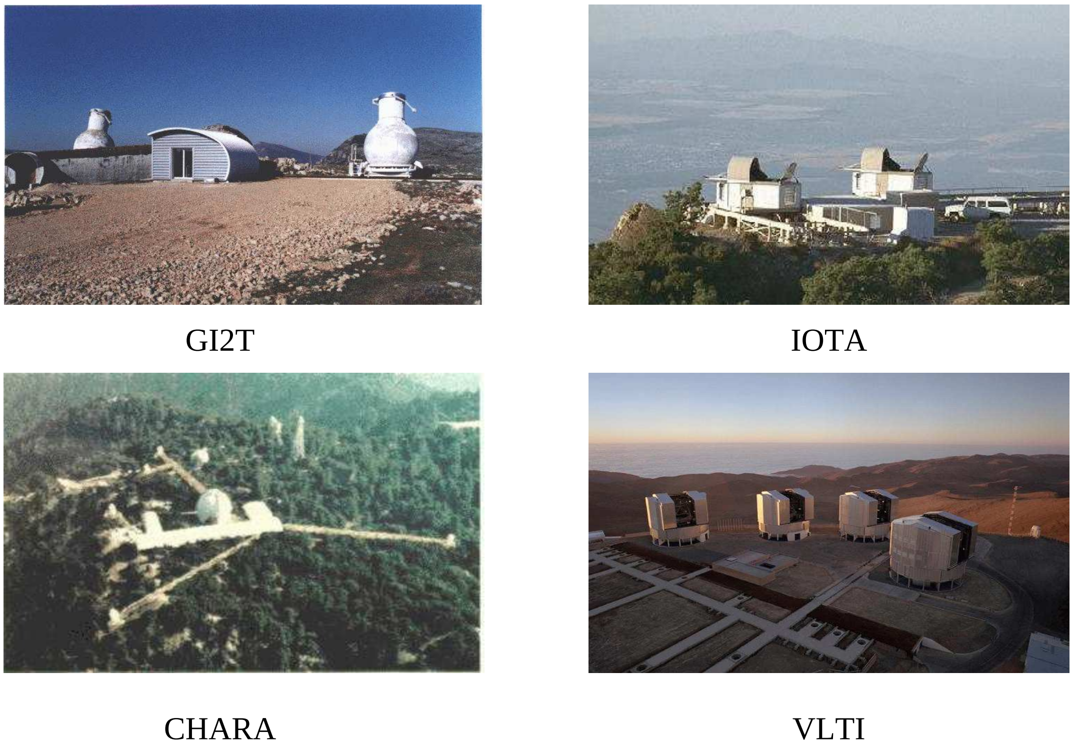

Figure 4.2: Four examples of optical interferometers. The array can be linear and continuous (GI2T), L-shaped with several stations (IOTA), Y-shaped with fixed telescopes (CHARA) or the filling of an equivalent 200-m aperture (VLTI).

- **Interferometric array**. Several types of array configurations have been designed in order to give access to the different spatial frequencies (see Fig. 4.2). The three criteria are the number of telescopes, but also the length and the orientation angle of their associated baselines. One can choose to have either fixed telescopes (PTI, KI, VLTI/VIMA) or movable telescopes (GI2T, IOTA, VLTI/VISA). Like in radio interferometry, Earth rotation allows to sample the uv tracks. If the object displays a wavelength-independant structure like a binary, the coverage of the uv plane can be performed with spatial frequencies at different wavelengths.

- **Apertures.** They ensure the light collection. Either siderostats (IOTA, PTI, SUSI) with diameter less than 50 cm or more or less traditional telescopes (GI2T, CHARA, KI, VLTI) for larger diameters can be used. In case of large siderostats, a fixed beam compressor is used to compress the beam diameter for propagation toward the central lab.

- **Beam transportation**. Once the object light has been captured by the apertures, one carries out the individual beams toward the combination laboratory. Usually the optical path is designed so that a complete symmetry of the mirrors in each arms minimizes the differential polarization effects. The optical train contains typically of the order of 20 mirrors. [Froehly 1981] suggested to use optical fibers to carry the light from the apertures to the lab. This technology has been tested by [Coudé Du Foresto, Mazé, & Ridgway 1993] and is the key of the coming O'HANA project which will gather the light from the 8-m class telescopes on the Maunea Kea in Hawaii [Perrin et al. 2000]. Some interferometers use vacuum optics (PTI, IOTA, NPOI,...) to decrease the dispersion due to the propagation in the air of the delayed beam (see Sect. 4.5.2).

- **Wavefront correction**. The incoming light travels through the atmospheric turbulence (see Sect. 4.5.1). The wavefront is then corrugated and the images of the object move due the *seeing*. Almost

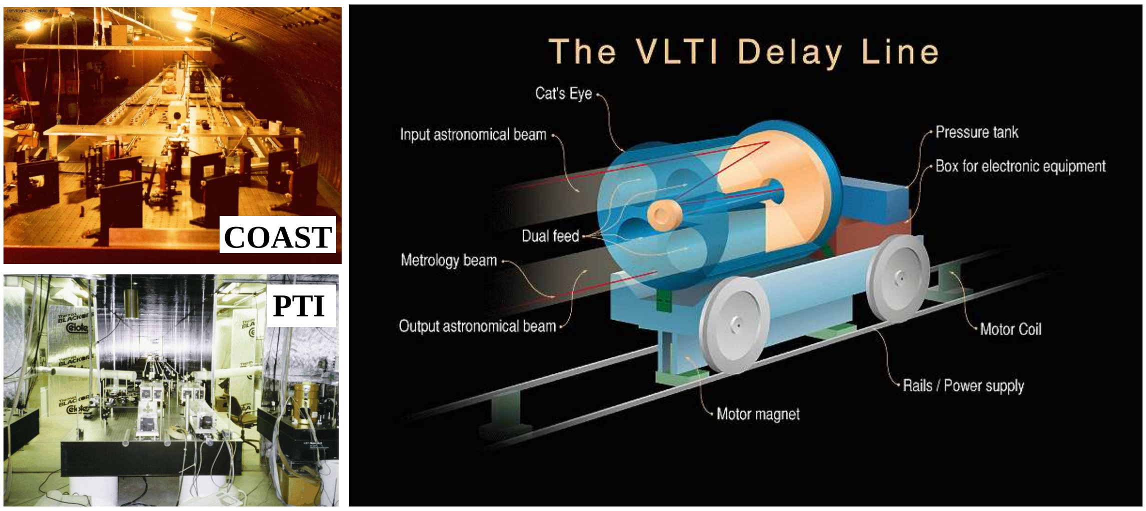

Figure 4.3: Some examples of delay lines

all interferometers have therefore at least a 2-actuator adaptive optics system that corrects from the tip and the tilt (IOTA, NPOI, PTI). Large interferometers with aperture diameter larger than 1 m have plans for higher correction of the wavefront (VLTI/VIMA, KI-main, GI2T, LBT, CHARA). The goal is to stabilize the light and to increase the Strehl ratio of individual beams, i.e. the quality of the central peak. One should note that GI2T currently works in multi-speckle mode and therefore does not formally require AO systems to properly work, even if it would increase its sensitivity performance.

- **Delay lines**. When the object observed is traveling across the sky, the external optical path difference (OPD) between two arms is equal to $\mathcal{B} \sin z$, where $\mathcal{B}$ is the baseline length and z is the zenith angle. To achieve the fringe detection, the two arms should be equal at the level of the micrometer. In the first experiment by [Labeyrie 1975], the stabilization of the OPD was performed by moving the beam combination table. Nowadays, most interferometers prefer to use optical delay lines (DL) using cat's eyes located on movable chart. Moving a DL either in one arm or another compensates the sidereal motion of the star, exactly like telescope mounts follow the stars displacements. For very long delays, one often has to design and build long DLs that offer only optical delays by steps of a few meters coupled with DLs with shorter strokes (KI, CHARA).

- **Optical path difference stabilization**. The atmospheric turbulence produces not only wavefront corrugation at the level of individual apertures but also at the level of the interferometer called atmospheric piston. The consequence is that the OPD is fluctuating and the fringes move back and forth. Using a fringe sensor (a simple beam combiner that measures the OPD at a frequency higher than the typical atmosphere timescale), one is able to send corrective commands to the DLs. This feature is the zero-degree of adaptive optics for an interferometer. A fringe sensor coupled with a DL is called a fringe tracker and allows to stabilize the signal for longer integration.

- **Beam combination**. The interferences between the various beams can be achieved in many ways (see Sect. 4.4). One usually distinguishes the so called co-axial beam combiners (BCs) that combine the light coming from the same optical axis (like with a beam splitter in the laboratory Michelson interferometer) and the multi-axial ones that produce interferences between beams coming from different directions (like in the Young's experiment). The beam combination is usually made with lenses, mirrors and/or beam splitters. However, the optical functions used by the telecommunication industry has given birth to fibered BCs (e.g. FLUOR [Coudé Du Foresto, Mazé, & Ridgway 1993]) and integrated optics ones (see IONIC experiment [Malbet et al. 1999]) using single mode waveg-

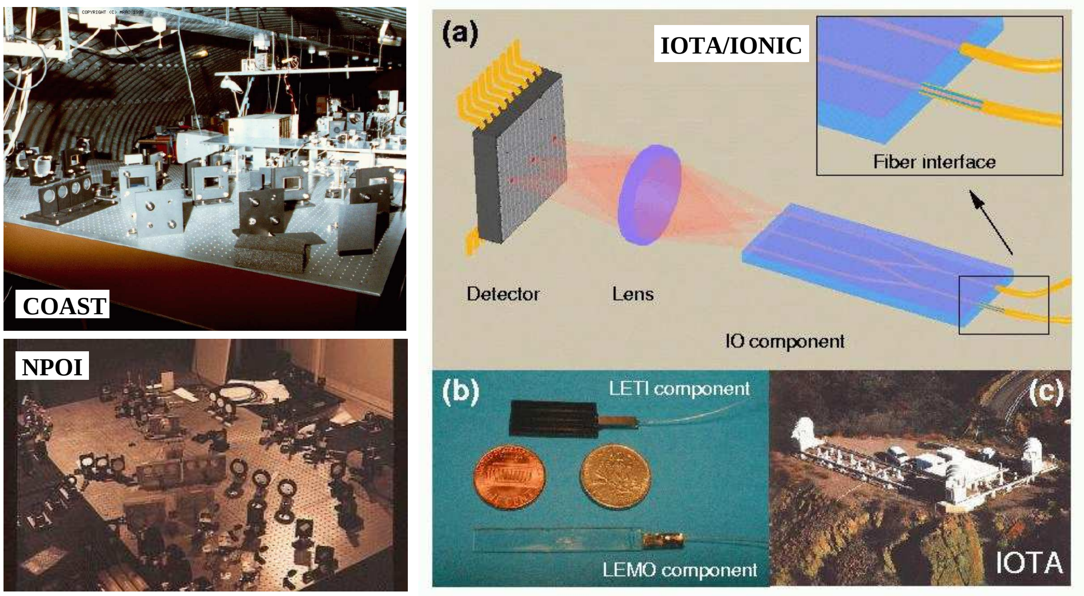

Figure 4.4: Beam combiners. Left: beam combiners in bulk optics. Right: beam combiners using the integrated optics technology.

uides.

- **Detection**. This fundamental step makes use of photon detector either with photo-counting capability in the visible range or CCD with low read-out noise in the infrared. The dispersion of the light can be done just before the detection and the instrument looks similar to a spectrograph.

The schematic layout of the VLTI is displayed on Fig. 4.5. It is typical of most of interferometers. A difference is that the focal plane hosts several instruments: VINCI the commissioning BC based on known technology, AMBER the near infrared spectrograph and MIDI the thermal infrared camera. Smaller interferometers have usually only one dedicated instrument optimized for their astrophysical targets (binaries, stellar diameters, envelopes,...).

4.3.2 Specific applications

I see 5 types of scientific usages of the interferometric light combination.

Interferometry in the past has been most often used with only **two apertures**. Therefore since the atmospheric piston prevents any absolute phase calibration, the astronomers can only measure the amplitude of the complex visibility and a phase difference between two spectral channels when the instrument has some spectroscopic capability. The goal is then to measure the visibility amplitude or a differential phase, also called two-color phase, and to interpret the variations of these measurements with time, with baseline length, or with baseline angle. An important field of application is the measure of stellar diameters and binary orbits, but recently it has been extended to circumstellar envelopes and accretion disks.

The dream of most interferometrists is to perform actual imaging like in the radio domain using **aperture synthesis**. The interferometer COAST has been built with this goal in mind. That is why it is composed of 4 telescopes in order to increase the efficiency of the uv plane coverage, but also to use the technique of closure phases. This closure phase technique, used to be of high importance in radio interferometry, allows to self-calibrate the sum of the phases measured simultaneously by three baselines. This method is very similar also to the bispectrum one in speckle interferometry. However for technical reasons, the beam combination of $N \geq 3$ beams appears to be difficult and only few reconstructed images

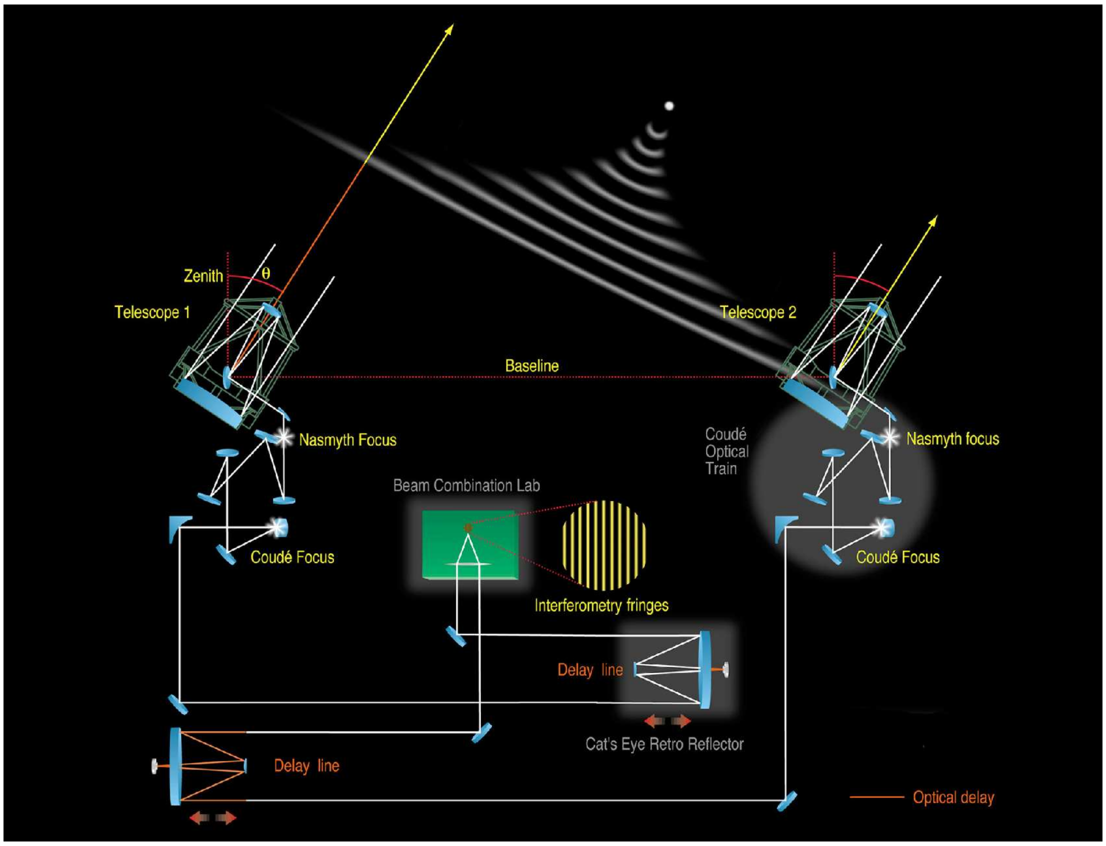

Figure 4.5: VLTI optical layout

have been obtained so far. The outcome of integrated optics might change the situation in the future [Malbet et al. 1999].

The group working on NPOI has been focusing on the **wide-angle astrometry** for a long time (previously at the Mark III interferometer, ancestor of PTI and NPOI). The idea is simple and once again similar to what is being done in radio: when the interferometer detects fringes, the two paths of the interferometer are equal to a fraction of a micrometer. Since the delay due to the sidereal motion of the stars is given by

$$\delta = \mathcal{B}\cos\theta + C, \tag{4.2}$$

where $\mathcal{B}$ is the length of the baseline, θ is the altitude of the star in the sky and C an internal constant, then the knowledge of $\mathcal{B}$ and C together with the measure of the stroke given to the DL give access to $\cos\theta$. The objective consists in measuring the group delay of several tens of stars at different moments of the night and to fit the curves with cosine of the same amplitude $\mathcal{B}$. The internal metrology measures the internal constant C. After post-processing, both the position of the stars and the baseline are deduced with a precision of the order of the fringe spacing $\lambda/\mathcal{B}$, i.e. about 1 mas.

Recently, following the work on Mark III, [Shao & Colavita 1992] proposed the **narrow-angle astrometry** technique. The idea is to observe two objects sufficiently close so that the atmospheric perturbations affecting the stellar path on each telescope is almost the same for the two objects. The correlations in the perturbations is used to increase the accuracy of astrometric measurements down to 10 μas opening the search for the reflex motion of stars due to the presence of planets. To achieve such an objective, one has to separate the field at each aperture in two sub-apertures and to propagate in parallel the light from the two stars in two different interferometric systems. A differential metrology allows to link the two interferometers. When the fringes are detected on the two detectors, the differential metrology gives the

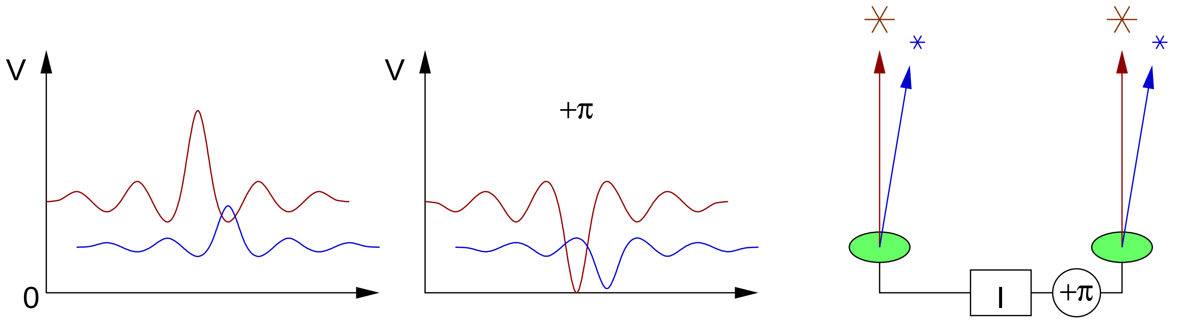

Figure 4.6: Principle of a nulling interferometer (see text for details).

differential delay between the two stars:

$$\Delta\delta = \mathcal{B}\Delta\theta + d, \tag{4.3}$$

Where $\Delta\theta$ and d are respectively the differential angle between the two stars and the internal constant. One interesting application of such a dual interferometer is **phase referencing** like in radio: if a close-by reference star has a zero-phase then the measure $\Delta\delta$ leads to the actual phase of the science target. In radio, the atmosphere is quiet enough to measure the phase reference by depointing the interferometer whereas in the optical domain, the two measurements must be made at the same time. The PTI is the interferometer that hosts this technique.

Finally, many groups are working on the concept of **nulling interferometers**. The idea [Bracewell 1978] is to use the coherence of the light to interferometrically cancel the light arriving in the interferometer boresight. An object located off-axis has translated fringes. In certain directions, the bright peaks of the object fringes are located over the dark zones of the central star fringes. If the nulling in the dark fringes is high enough, the dynamic range of this technique can reach high values (see Fig. 4.6). This application is extremely interesting in the case of the study of extra-solar planets. Those planets are expected to be between 10^4 and 10^9 fainter than their parent stars. Nulling the light of the central star is the only way to detect photons from these worlds. To achieve such performances, the instruments like DARWIN pill up several stages of such nulling interferometers to reach high rejection rate.

4.4 Formation of the interferometric fringes

In this section, I focus on the light combination and the signal detection.

4.4.1 Beam combination

[Mariotti et al. 1992] tried to classify the different types of beam combination (see Fig. 4.7). They have defined 4 levels of criteria:

- **Beam étendue:** what is the field accessible by the detector at each telescope? If this field is limited to the diffraction pattern of the telescope, then the interferometer is called *single-mode*, whereas if the interferometer processes more information than the one in the diffraction pattern it is *multi-mode*. For example in radio, all interferometers are single-mode.

- **Beam direction:** how the light coming from the different arms are combined? If the beams are combined with beam splitters so that they appear to come from the same direction, then the combination is called *co-axial* (see Fig. 4.8a) and gives a flat tint on the detector. If the beams appear to come from various direction (see Fig. 4.8b) like in the Young's experiment the beam combination is called *multi-axial*.

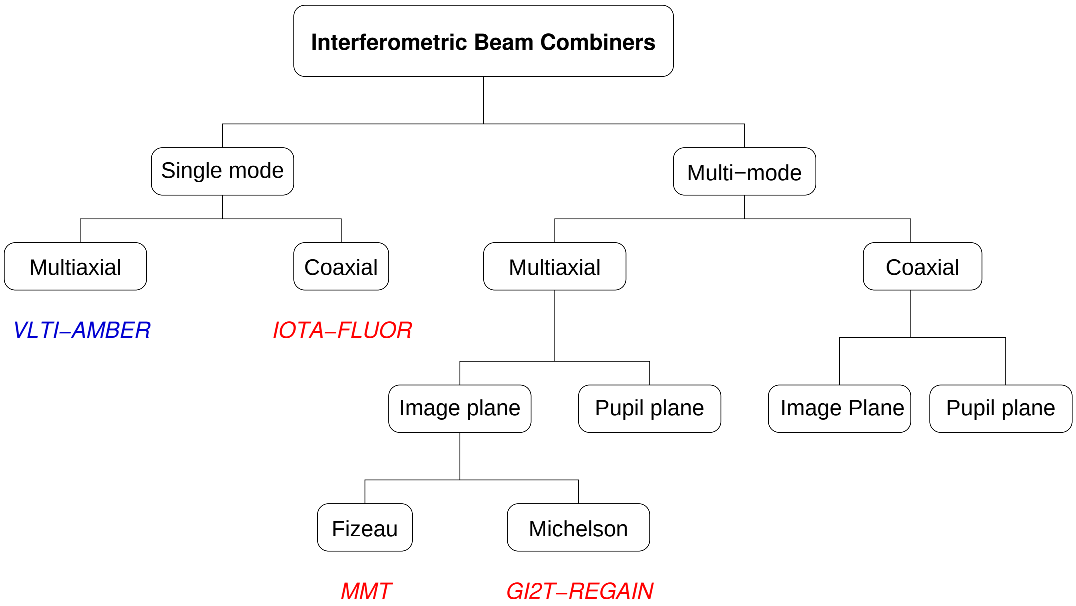

Figure 4.7: Mariotti's classification (adapted from [Mariotti et al. 1992]).

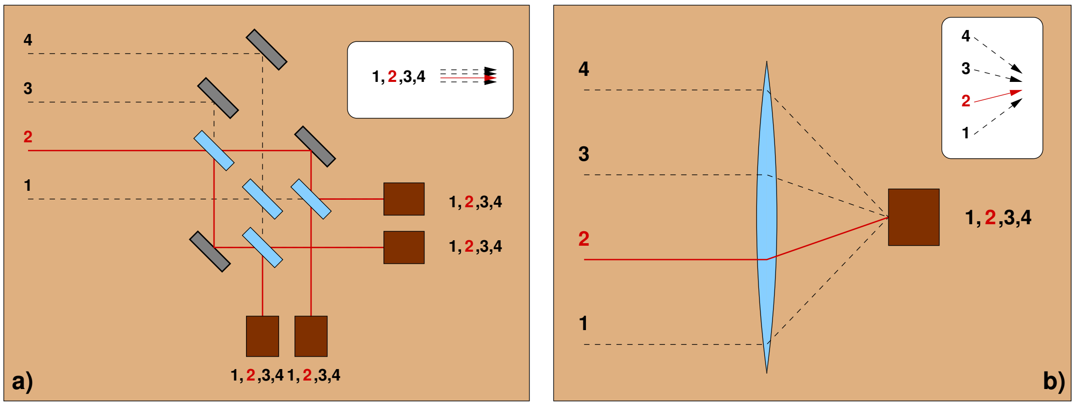

Figure 4.8: All-in-one coaxial (left) and multiaxial (right) 4-way beam combination schemes.

- **Combination plane:** does the beam combination occur in the *image plane*, conjugated with the sky, or, in the *pupil plane*, conjugated with the telescope pupils (see Fig. 4.9)?
- **Relation between the input and output pupils:** what is the interferometric field of view? The answer depends on the relationship between the input / output[1] pupil geometry. One can distinguish 3 cases:
  1. *Fizeau-Stéphan* setup where the input and output pupils are homothetic (both pupil separation and diameters).
  2. *Densified pupil* used by the hyper-telescopes [Pedretti et al. 2000] where the position of the sub-pupils in the output pupil are scaled to the input ones but the diameters of the sub-pupils are magnified.
  3. *Michelson-Pease* setup where there is no link between the input pupils and the output pupils.

  The resulting field of view (FoV) are sorted by increasing size: $FoV_1 \geq FoV_2 \geq FoV_3$. The Fizeau-Stéphan set-up gives access to a larger field of view but is difficult to implement since the homethetic relation must be conserved during the transit of the object. It would require continuously reconfigurable beam combiners.

The tree that corresponds to this classification (see Fig. 4.7) shows the complexity of beam combination in optical interferometry. However, all but one current interferometers have been designed to be single-mode, GI2T-REGAIN being the only one using the multi-mode beam combination scheme.

4.4.2 Fringe coding and detection

Once the beams have been combined, one still needs to detect the fringes. Since optical detectors have access only to the intensity of the electric field, the signal must be modulated in phase in order to measure both the amplitude and the phase of the visibility. The signal measured from the combination of two arms A and B is deduced from Eq. (4.1):

$$I(\phi_{\mathrm{mod}}) = I_A + I_B + 2\sqrt{I_A I_B}\, V_O V_I \;\cos(\phi_O + \phi_{\mathrm{mod}}). \tag{4.4}$$

The goal is to evaluate the complex visibility $V_O \exp(i\phi_O)$ of the object. One needs to modulate ϕ_{mod} so that the variation of $I(\phi_{\mathrm{mod}})$ in function of ϕ_{mod} leads to the amplitude of the visibility. There are mainly two types of fringe coding: the temporal or spatial coding.

In the multiaxial combination scheme, since the beams from the different arms come from different directions, $\phi_{\mathrm{mod}}(x) = 2\pi(bx/d)/\lambda$. Therefore analyzing the light at different positions on the detector plane, gives the visibility information (see Fig. 4.10). In the coaxial combination scheme, one introduces a variable optical path length on one arm: $\phi_{\mathrm{mod}}(\delta) = 2\pi\delta/\lambda$ (see Fig. 4.11). There exists also other types of coding using the polarization or wavelength dependence of the phase, but they are rarely used.

When combining more than two beams, one has to decide if one uses all-in-one or pairwise beam combination. When the number N of telescopes increases the all-in-one combination is prefered because it involves less optical elements. In a pairwise scheme, all beams must be splitted in $N-1$ beamlets to be combined with the other telescopes. The all-in-one solution is displayed both for co-axial and multi-axial combinations in Fig. 4.8. However, one has to be cautious on the redundancy of the fringe frequencies so that the signals from two different baselines are not mixed together. That is why in the multi-axial combination the sub-pupils are separated by non-redundant separations, and, in co-axial combination the OPD scan frequencies and amplitudes are also not redundant.

4.5 Main challenges in interferometry

In this section, I address the main difficulties encountered in optical interferometry. The main one is the effect of turbulence due to the atmosphere. I will also tackle the limitation in terms of performance due to the various types of noise.

[1] The input pupil is the plane where the electric field coming from the object enters the interferometer. The output pupil is the plane where the electric field exiting from each optical train before being combined on the detector.

4.5.1 Atmosphere turbulence

The main effect of the presence of the atmosphere is the corrugation of the incoming wavefronts. Due to difference of temperature between the ground and the upper layers of the atmosphere, convection occurs and creates turbulent eddies. These eddies are characterized by different temperature and therefore different refractive indices. They move up and down with different spatial scales. When looking to objects through the atmosphere, the light rays are deviated randomly, i.e. the plane incoming wavefront is corrugated by different phase delays depending on the total optical thickness of the atmosphere along the propagation path (see Fig. 4.12). In optical interferometry, this phenomenon called *seeing* yield two main consequences:

- at each telescope pupil entrance, the **local wavefront is corrugated**. One does not get diffraction-limited images of the object, but seeing-limited ones. In short exposure images and for multi-mode interferometers, the image is formed of various speckles (see left panel of Fig. 4.13) and in long-exposure images its typical size is given by the characteristic size of turbulent cells where the light is coherent, i.e. several tenths of meters. In addition, these features move with time at timescale of several milliseconds. In the case of single-mode interferometers, the speckles are spatially filtered at the entrance of the interferometer and are translated in fluctuations of the light coupling. Therefore one has to correct from the photometric fluctuations induced by the turbulence (see right part of Fig. 4.13 and Sect. 4.5.3).
- the atmosphere induces **fluctuations of the optical path differences** for each baseline. The result is that the fringes are not stable at a given optical delay but randomly move around the sidereal position. It is impossible to calibrate the phase of the fringes and their amplitude is also decreased due to smearing during the integration time.

The atmosphere decorrelates the phase between different points of the incoming wavefronts both in space and in time. That is why we usually present the turbulence as yielding coherence volumes inside which the wavefront can be considered as a non-disturbed plane wave. The geometric parameters of the coherence cell are called the Fried's parameters:

- the size of the cell, r_0, typically 10 cm at $\lambda = 0.5\ \mu$m and 1 m at $\lambda = 2.5\ \mu$m depending of the turbulence strength.
- the coherence time, t_0, typically 10 ms at $\lambda = 0.5\ \mu$m and 100 ms at $\lambda = 2.5\ \mu$m.

The turbulence occurs at different spatial scales and a popular model is the Kolmogorov model that represents the power spectrum of the turbulence as a power law [Roddier 1981]. However the turbulence at small spatial frequencies saturates, i.e. the size of the largest eddies is limited. This limit, L is called the outer scale of the turbulence and is important in interferometry since we estimate its size to be of the order of $10 - 100$ m, typical lengths of most interferometer baselines. If the baseline is larger than the outer scale then the effect of turbulence is less than predicted by the Kolmogorov model.

4.5.2 Other atmosphere systematics

Optical interferometers must also take into account the atmospheric **refraction** and the **longitudinal spectral dispersion**.

The wavelength dependence of the air refractive index implies wavelength-dependent refraction angles when the light enters the atmosphere. The atmosphere acts like a prism and the images at each aperture are spectrally dispersed. Single mode interferometers spatially filter the incoming wavefront, that means they select a part of the image. Therefore this refraction effect decreases the coupling factor in the interferometer. The larger the telescope size, the smaller the diffraction-limited images: this effect begins to be important for large telescopes. **Atmospheric dispersion correctors** are classical devices made of two prisms that can rotate and compensate the dispersion due to the atmosphere refraction.

The refraction induces chromatic arrival angle, but does it result in chromatic OPD. Fig. 4.15 shows that even if the optical paths are different for two different wavelengths, they are the same for each aperture and the OPD remains zero for all wavelengths. The refraction does not yield a chromatic OPD.

However, the optical delay due to the zenith angle of the observed object has to be compensated by delay lines. If the delay lines are located in vacuum the compensation matches exactly the geometrical delay above the atmosphere, but if the optical delay in performed in air, then the compensation is performed only for one wavelength because of the chromatism of the air refractive index $n(\lambda)$. The resulting OPD given by a delay L of the delay line that matches the geometrical delay δ at $\lambda = \lambda_0$ is then:

$$OPD(\lambda) = \left(\frac{n(\lambda)}{n(\lambda_0)} - 1\right)\delta \tag{4.5}$$

Therefore the location of the zero-OPD changes with wavelength. At high spectral resolution, the main effect is to twist the fringes, whereas at low spectral dispersion the contrast of the fringes can be severely decreased. To overcome this effect and besides using vacuum delay lines, two translating prisms produce a variable glass thickness that compensates exactly the chromatic OPD. This device is called a **longitudinal dispersion compensator**.

4.5.3 Fighting the atmosphere: complexity and accuracy

The previous sections show that the propagation in the air implies several problems. The chromatic effect of the air refractive index can be compensated by an atmospheric dispersion compensator and a longitudinal dispersion corrector. These phenomena are completely predictable and therefore can easily be controlled by computer in function of the zenith angle.

However the effect of the turbulence is much more difficult to control since the time scale is of the order of several milliseconds and the spatial scales are small. Adaptive optics (or tip-tilt compensation) and fringe trackers are therefore required to increase the sensitivity of optical interferometers (see Sect. 4.3). However the correction is never perfect and some residuals can still affect the signal.

One solution is to use speckle techniques to calibrate those residuals. GI2T has proven that one can use several speckles to calibrate the visibility of an object. Another method is to filter out the incoming wavefront. The principle is well-known by the opticians: they clean up images by placing so-called *spatial filters* in the Fourier plane associated to the images. With a pinhole at the focus of a telescope, the wavefront in the exit pupil is then cleaned up and flat. The wavefront corrugation is transfered in intensity fluctuations since the speckle image on the pinhole is not stable. Optical waveguides, like optical fibers, are optical devices that behave like infinitively small pinholes but with a high coupling efficiency (typically 70%). The signal that exits from a waveguide is an electric field whose shape is given by the geometry of the waveguide (and therefore is fixed) and for which only two parameters can vary: the global amplitude and the phase. By measuring the variations for the photometry for each beam, we can compute a visibility corrected from the atmospheric perturbations. The visibility estimator,

$$V_{\mathrm{corr}} = \frac{2\sqrt{I_A\,I_B}}{I_A + I_B}\,V_{\mathrm{mes}}, \tag{4.6}$$

little depends on the turbulence with V_{mes} the raw visibility, I_A and I_B the intensities measured for each beam.

This method has proven to be very accurate in measuring visibilities. FLUOR reaches 0.3% for some targets [Coudé Du Foresto, Ridgway, & Mariotti 1997]. However, one should keep in mind that the measured visibility is not exactly the object visibility except if the objet is not resolved by the individual apertures. When the object is larger than the projected size of the spatial filter on the sky, one has to apply a visibility correction using the information given by the image obtained with the resolution of the individual apertures.

4.5.4 Noise sources - Sensitivity

The signal measured with an optical interferometer is affected by several sources of noises. In the case of the instrument AMBER on the VLTI these sources of noises are:

- the **photon noise** is the fundamental noise associated to the detection of the photons. It follows a Poisson-type statistics.

– the **detector read-out noise** is the noise of the electronics that reads the signal. It is an additive Gaussian noise with a characteristic level called the read-out noise (RON).

– the **thermal noise** is the noise that comes from the detection of background photons. The background level is measured and subtracted. The background estimation gives an error due to the photon statistics.

– the **instrument OPD stability** is not a noise that affects the detected photons, but the measured visibility. The residual motions of the optics in the instrument induce a blurring of the fringes at a small level. In AMBER, we expect this level to be lower than 10^{-4} of the unit visibility.

– the **atmosphere fluctuations**, even corrected by simultaneous measurements of the photometry induce degradation of the signal-to-noise ratio. The obvious situation is the case where no photons are coupled into the interferometer.

Computing the error propagation in the final signal allows to calculate a signal-to-noise ratio (SNR) for different type of situations. To illustrate the consequence of the source brightness on the performance of an interferometer, I show in Fig. 4.17 the SNR curve for different star magnitudes in the case of the AMBER instrument on the unit telescope of the VLTI with different typical values of the site.

For bright objects the dominant noise source is the instrument stability. When observing faintest objects, the limitations become first the photon noise, then depending on the integration time, either the thermal background noise or the read-out noise.

4.6 Conclusion

I have presented some elements of the present state of the art in optical interferometry focusing on the functional description, some design choices and the various limitations with the objective to give to the readers the keys to compare this technique with radio interferometry at millimeter wavelengths.

We see that optical interferometry is a younger technique than the radio interferometry because of the complexity of the systems mainly due to the struggle against the atmosphere. It leads to smaller spatial resolution but has still to learn from the radio experience.

We are entering a new era where optical interferometers with large telescopes and increased sensitivity become general user instruments (KI, VLTI). I did not address the topic of optical interferometry in space that faces other challenges. However the search for extra-solar terrestrial planets is certainly driving this area with two main projects: the Space Interferometry Mission (SIM) dedicated to astrometry and the TPF/DARWIN mission focused on nulling interferometry.

Note: To obtain exhaustive and todate information on optical interferometers, I advise the reader to browse **OLBIN**, the **optical long baseline interferometry newsletter** managed by P. Lawson. The address is `http://olbin.jpl.nasa.gov`.

Figure credits

Fig. 4.1: L. Rarogiewicz, Mount Wilson Observatory.

Fig. 4.2: Département Fresnel, Observatoire de la Côte d'Azur; Smithsonian Astrophysical Observatory and Harvard University Center for Astrophysics, University of Massachusetts; Georgia State University; European Southern Observatory.

Fig. 4.3: Mullard Radio Astronomy Observatory, University of Cambridge; Jet Propulsion Laboratory, Palomar Observatory; European Southern Observatory.

Fig. 4.4: Mullard Radio Astronomy Observatory, University of Cambridge; US Naval Observatory, Naval Research Laboratory, Lowell Observatory; Laboratoire d'Astrophysique, Observatoire de Grenoble.

Fig. 4.5: European Southern Observatory.

Fig. 4.7: European Southern Observatory [Mariotti et al. 1992].

Fig. 4.10: right panel, Infrared Interferometry Group, Max-Planck Institut für Radioastronomie.

Fig. 4.11: right figure, Laboratoire d'Astrophysique, Observatoire de Grenoble.

Fig. 4.13: Annual review of astronomy and astrophysics [Labeyrie 1978]; Laboratoire d'Astrophysique, Observatoire de Grenoble.

Fig. 4.14: AMBER consortium OCA, LAOG, UNSA, MPIfR, OAA (AMB-OSM-007 report).

Fig. 4.16: Astronomy & Astrophysics Supplement Series, EDP Sciences [Coudé Du Foresto, Ridgway, & Mariotti 1997]; DESPA, Observatoire de Paris-Meudon.

Fig. 4.17: AMBER consortium OCA, LAOG, UNSA, MPIfR, OAA (Instrument Analysis PDR Report).

Internet resources

The following web sites have been used for some figures of this chapter.

- Mount Wilson Observatory, 20ft interferometer: `http://www.mtwilson.edu/Tour/100inch/20ftI` (Fig. 4.1)
- GI2T: `http://www.obs-nice.fr/fresnel/gi2t` (Fig. 4.2)
- IOTA: `http://cfa-www.harvard.edu/IOTA` (Fig. 4.2)
- CHARA: `http://www.chara.gsu.edu/CHARA` (Fig. 4.2)
- VLTI: `http://www.eso.org/projects/vlti` (Figs. 4.2, 4.3, 4.5)
- COAST: `http://www.mrao.cam.ac.uk/telescopes/coast` (Figs. 4.3, 4.4)
- PTI: `http://huey.jpl.nasa.gov/palomar` (Fig. 4.3)
- NPOI: `http://ad.usno.navy.mil/npoi` (Fig. 4.4)
- IONIC: `http://www-laog.obs.ujf-grenoble.fr/activites/hra/ionic` (Figs. 4.4, 4.13)
- MPIfR: `http://www.mpifr-bonn.mpg.de/div/ir-interferometry` (Fig. 4.10)
- AMBER: `http://www.obs-nice.fr/amber` (Figs. 4.14, 4.17)
- FLUOR: `http://despa.obspm.fr/fluor` (Fig. 4.16)

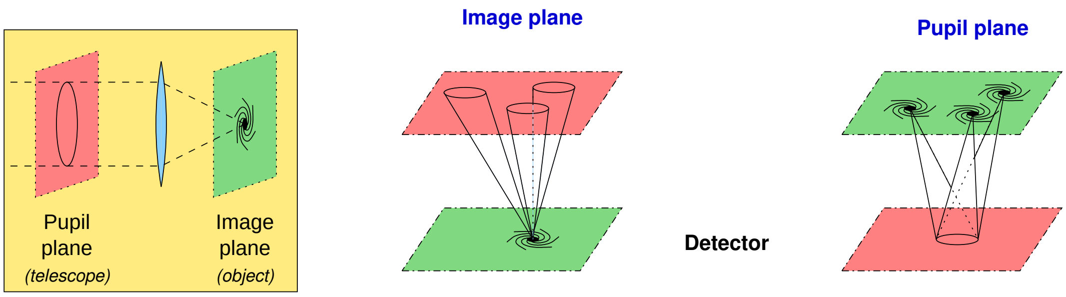

Figure 4.9: Combination planes.

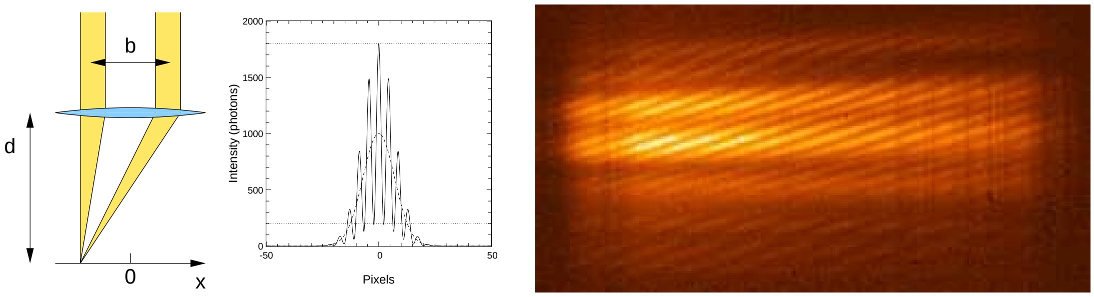

Figure 4.10: Multiaxial beam combination and spatial coding of two-aperture fringes. Left: the OPD changes with the x-position on the detector. Center: the fringes appear superposed to the beam shape. Right: fringes (y-axis) spectrally dispersed (x-axis) in the IR channel of GI2T [Weigelt et al. 2000].

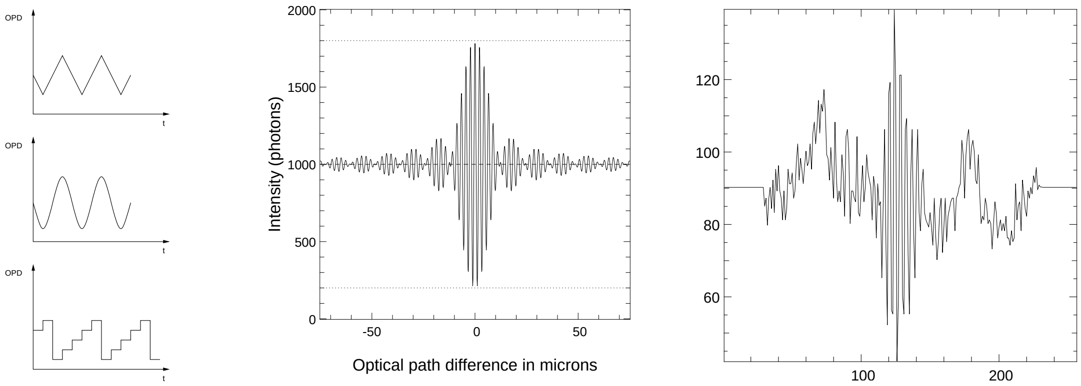

Figure 4.11: Coaxial beam combination and temporal coding of two-aperture fringes. Left: different types of OPD modulation. Center: theoretical signal. Right: signal observed with the IR table at IOTA.

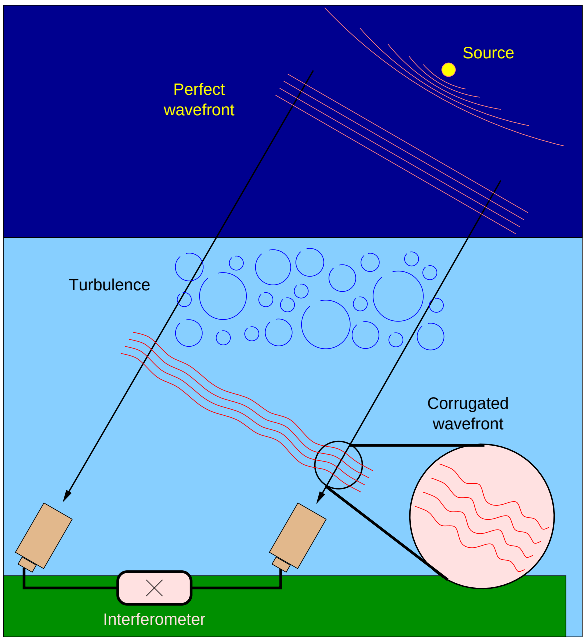

Figure 4.12: Effect of the atmosphere turbulence on the incoming wavefronts.

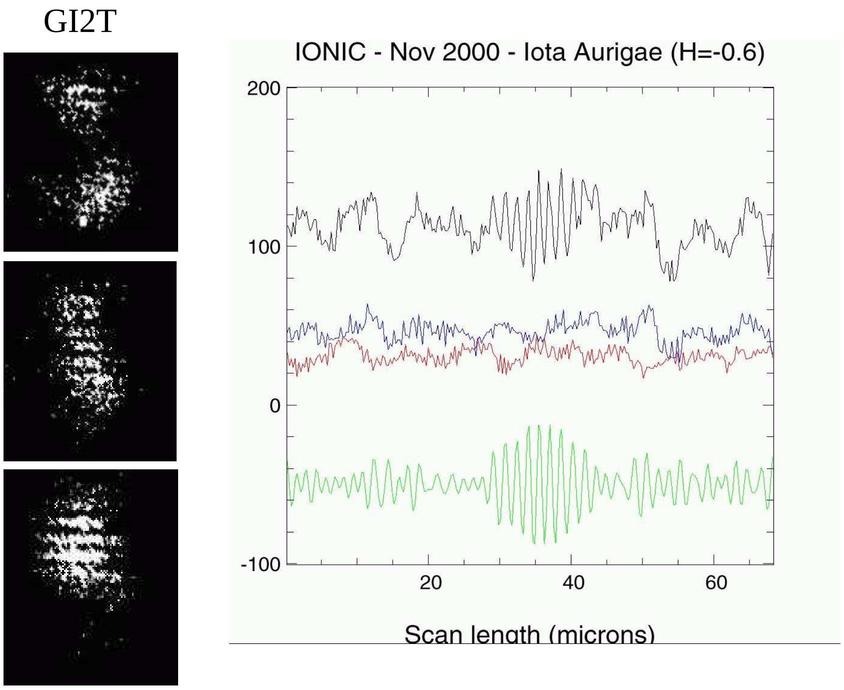

Figure 4.13: Effect of the turbulence of each aperture. Left: in multi-mode beam combination, the image is formed of speckles with fringes at different phases (GI2T, adapted from [Labeyrie 1978]). Right: in single-mode beam combination, the wavefront corrugation is translated into photometric fluctuations (IONIC, [Berger et al. 2001]). Upper curve: raw interferometric signal; center curves: photometric signals; lower curve: photometry-corrected interferometric signal (see also Sect. 4.5.3)

.

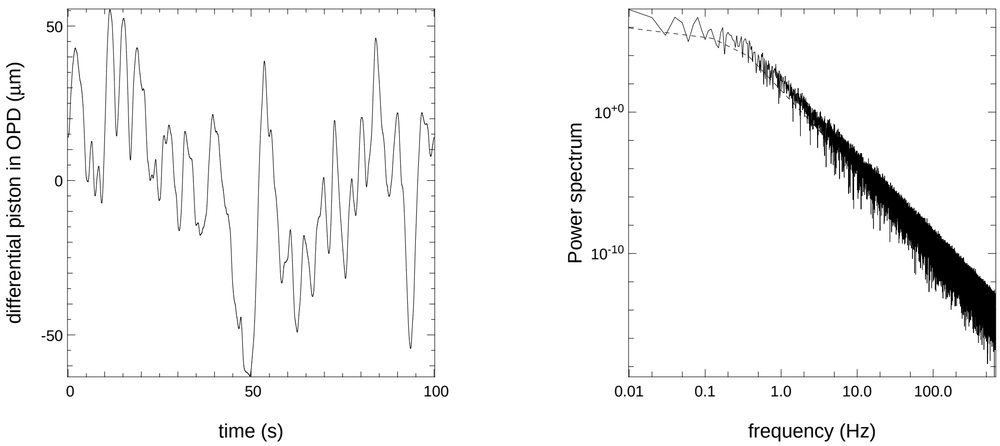

Figure 4.14: Optical path fluctuations due to the turbulence. Left: simulations of the fluctuations for two Unit Telescopes at the VLTI with typical seeing parameters (in microns). Right: the power spectrum of the fluctuations follows a Kolmogorov law with a saturation at low frequency due to the outer scale.

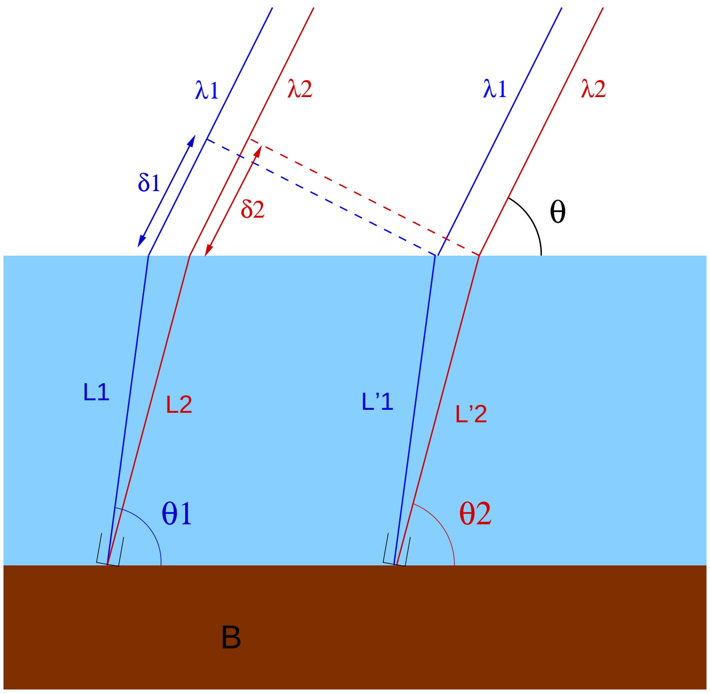

Figure 4.15: Effect of the atmosphere refraction. The object image at each telescope entrance is in fact a small spectrum. However there is no effects on the optical delay since the optical path for the two beams in the atmosphere is the same at each wavelength λ_1 and λ_2, and, the resulting OPD does not depend on wavelength. Even if $L_1 \neq L_2$, we have $L_1 = L'_1$ and $L_2 = L'_2$, and $\delta_1 = \delta_2$.

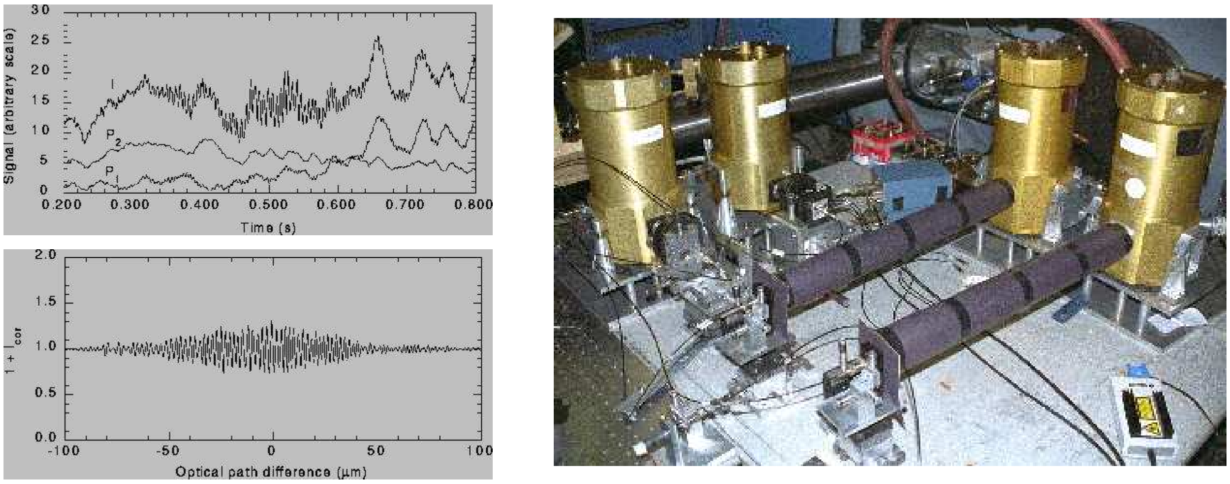

Figure 4.16: The FLUOR fiber beam combiner (right). Example of incoming signals: left top panel shows the raw signal with two photometry channels that monitors the coupling in the fibers; left bottom panels shows the corrected interferogram from [Coudé Du Foresto, Ridgway, & Mariotti 1997].

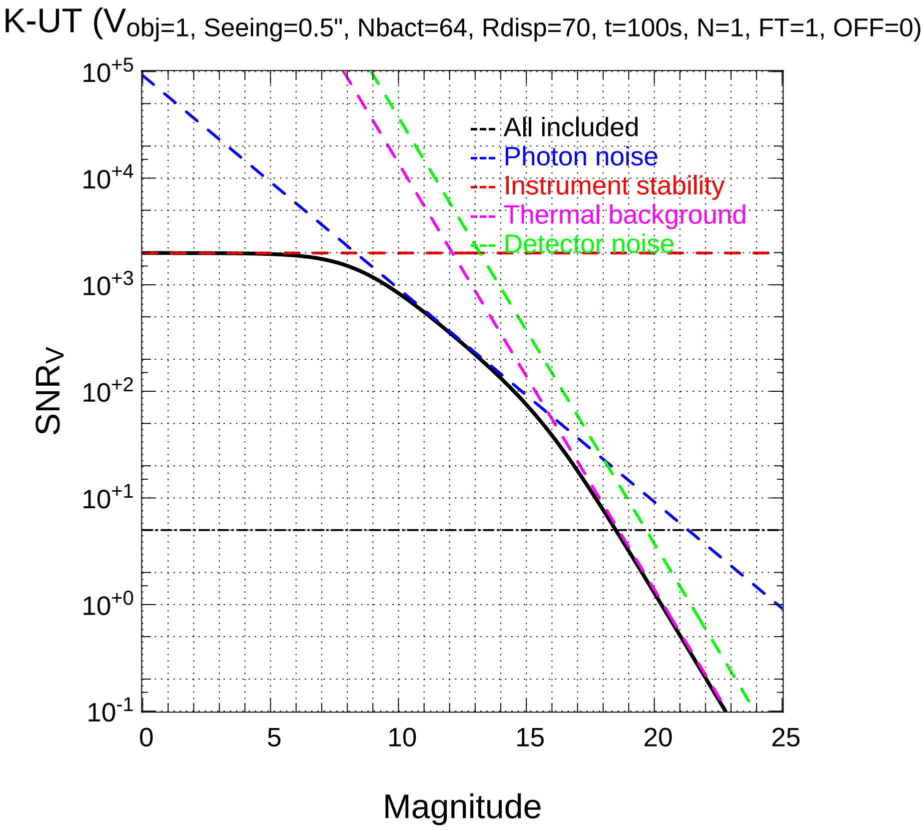

Figure 4.17: Signal-to-noise ratio computed for the AMBER instrument at the VLTI in the K band (2.2 μm) for an object of visibility of 1, a seeing of 0.5", a low dispersion, and a long exposure using fringe tracking.